



Deposition behaviors and interfacial interaction mechanism between carboxyl-modified polystyrene nanoplastics and magnetite in aquatic environment

Meimei Ran^{a,b}, Xin Nie^b, Jingxin Wang^c, Ruiyin Xie^{b,c}, Xiaoping Lin^{b,c}, Hanjun Zhu^b, Quan Wan^b, Yuhong Fu^{a,*}

^a School of Geography and Environmental Sciences, Guizhou Normal University, Guiyang 550025, China

^b State Key Laboratory of Ore Deposit Geochemistry, Research Center of Ecological Environment and Resource Utilization, Institute of Geochemistry, Chinese Academy of Sciences, Guiyang 550081, China

^c Guangdong Provincial Engineering Research Center of Public Health Detection and Assessment, School of Public Health, Guangdong Pharmaceutical University, Guangzhou 510310, China

ARTICLE INFO

Edited by Dr. HAO ZHU

Keywords:

Nanoplastics
Magnetite
Deposition
Interfacial interaction
Organic macromolecules

ABSTRACT

In aquatic environments, the deposition behaviors of nanoplastics (NPs) are closely associated with interfacial interaction between NPs and iron (hydr)oxides minerals, which are typically coupled with solution chemistry and organic matter. However, the roles of solution chemistry and organic matter in the deposition behavior of NPs with iron (hydr)oxides minerals and related interfacial interaction mechanism are still poorly understood. In this study, the deposition behaviors of carboxyl-modified polystyrene nanoparticles (COOH-PSNPs) with magnetite were systematically investigated. The results showed that electrostatic attraction, hydrogen bond, and charge-assisted hydrogen bond (CAHB) were the main forces for the deposition and interfacial interaction mechanism between COOH-PSNPs and magnetite. Increasing pH could significantly inhibit the deposition of COOH-PSNPs with magnetite. At pH 6.5, phosphate and dichromate significantly inhibited the deposition of COOH-PSNPs since their competitive adsorption for the surface sites on magnetite led to a potential reversal of magnetite, resulting in the strong electrostatic repulsion between COOH-PSNPs and magnetite. Moreover, when the concentration of phosphate exceeded 0.01 mM, the deposition of COOH-PSNPs was completely hindered. Organic macromolecules (OMs) markedly inhibited the interfacial interaction and deposition of COOH-PSNPs with magnetite by enhancing the electrostatic repulsion and steric hindrance between COOH-PSNPs and magnetite due to the formation of magnetite-OM associations. The inhibition abilities followed the order sodium alginate (0.1 mM) > humic acid (0.2 mM) > bovine serum albumin (5 mM). This study may provide insights for better understanding of environmental behaviors of COOH-PSNPs associated with magnetite and organic matter in natural environments at the molecular level.

1. Introduction

Plastic products are widely used in industrial production and daily life because of their low cost, durability, and easy of manufacture (Mamun et al., 2023; Huang et al., 2022). According to statistics, the global plastic production greatly increased from 1.5 million tons in 1950 to nearly 376 million tons in 2020, and it is expected to double in the next 20 years (Zhang et al., 2022a; Huang et al., 2021). However, only 6–26 % of plastics wastes were recycled, which means that most of plastics entered the environment (Zandieh and Liu, 2022; Zhang et al.,

2020). Large plastic waste fragments can decompose into small fragments or particles through physical, chemical, and biological degradation processes in the environment (Zandieh and Liu, 2022; Zhang et al., 2020), and further degraded into microplastics (MPs; 1 μm - 5 mm) and nanoplastics (NPs; < 1 μm) (Gigault et al., 2018; Nie et al., 2023; Sobhani et al., 2020; Gaylarde et al., 2021). Micro/nano plastics (M/NPs) can be absorbed by organisms and cells, and may be accumulated through the food chain, and may even be transferred to a higher trophic level, like humans (Schmidtmann et al., 2022; Wardrop et al., 2016; Chae et al., 2018). Compared with MPs, NPs have larger specific surface

* Corresponding author.

E-mail address: fuyuhong24@163.com (Y. Fu).

<https://doi.org/10.1016/j.ecoenv.2024.117608>

Received 31 July 2024; Received in revised form 18 November 2024; Accepted 21 December 2024

Available online 28 December 2024

0147-6513/© 2024 The Authors. Published by Elsevier Inc. This is an open access article under the CC BY-NC-ND license (<http://creativecommons.org/licenses/by-nc-nd/4.0/>).

area, higher mobility, abundant surface functional groups, and higher surface reactivity. Thus, NPs not only have higher adsorption capacity for pollutants, but they can also cross biological barriers, which may lead to more complex toxic effects to organisms and humans (Gaylarde et al., 2021; Bellingeri et al., 2020). Therefore, understanding the environmental behaviors of NPs is of vital importance for predicting their ecological risks.

The aggregation and deposition behaviors of NPs would affect their transport, fate, and ecological risk in aquatic environments, which are commonly influenced by their original physicochemical properties, solution chemistry (such as pH, ionic strength, and anions or cations), and coexisting organic matter as well as minerals (Huang et al., 2022; Xie et al., 2023; Li et al., 2019, 2021a). Previous studies have shown that natural minerals have high affinity for NPs due to their large surface area and abundant surface functional groups (Nie et al., 2023; Xie et al., 2023; Lin et al., 2024). As important components in sediments and soils, iron (hydr)oxides minerals are the most common minerals in natural environment, which can interact with various components in the environment due to their variable surface charge, high specific surface area, and surface reactivity (Bao et al., 2021; Vindedahl et al., 2016), and they have been proven to play important roles in the transport, deposition, and fate of NPs (Zandieh and Liu, 2022; Zhang et al., 2020; Nie et al., 2023). Thus, understanding the interfacial interaction mechanism between NPs and iron (hydr)oxides minerals is crucial for assessing the environmental behavior of NPs. Previous works have systematically studied deposition behaviors of NPs with various iron (hydr)oxides minerals (e.g., ferrihydrite, goethite, hematite, and magnetite), and gained some fundamental understanding of their interfacial interaction mechanisms (Nie et al., 2023; Xie et al., 2023). However, more detailed investigations are desired to fundamentally understand the effects of hydrochemical factors in environmentally relevant conditions. As one of the most common iron (hydr)oxides minerals in soils and sediments, magnetite (Fe_3O_4) has high reaction activity, abundant surface groups, and high surface area (Lin et al., 2021; Hu et al., 2021). Therefore, it could readily aggregate with NPs and cause the deposition of NPs. The strong magnetism of magnetite makes it easy to separate, making it applicable for removal of NPs via magnetic separation. Furthermore, organic matters such as humic substance, polysaccharide, and protein, which are commonly present in natural environments, can strongly interact with both NPs and iron (hydr)oxides minerals through electrostatic interaction, hydrogen bonding, van der Waals forces, ligand exchange, and steric forces, leading to the changes of surface properties and reactivity for both NPs and iron (hydr)oxides, which may greatly affect the environmental behaviors and toxicity of NPs (Xie et al., 2023; Zhang et al., 2019; Zhao et al., 2011). In addition, the formation of mineral-organic matter associations and their characteristics is strongly associated with molecular structure of organic matter. However, a molecular-level understanding of the effects of solution chemistry and various types of organic matter on the interfacial interaction mechanisms between NPs and magnetite at environmentally relevant conditions remains scarce, and the existing studies are not sufficient to elucidate the deposition mechanisms of NPs with magnetite under conditions similar to the actual aquatic environment, especially in the presence of various ions and complex organic macromolecules (OMs).

Polystyrene nanoplastics are one of the most common NPs in the environment. They will ineluctably undergo various aging processes to change their physical and chemical properties (such as increasing surface oxygen-containing functional groups and surface negative charges, etc.), thus affecting their environmental behaviors (Kong et al., 2023; Wang et al., 2023a; Shao et al., 2022; Zhang et al., 2022b; Dong et al., 2024; Yan et al., 2024). Consequently, in this study, carboxyl-modified polystyrene nanoparticles (COOH-PSNPs) were selected as representative aged NPs. The effects of solution chemistry (including pH, temperature, ionic type, and phosphate concentration) and OMs (including humic acid (HA), sodium alginate (SA), and bovine serum albumin (BSA)) on the deposition of COOH-PSNPs with magnetite were

systematically studied. The interfacial interaction mechanism between COOH-PSNPs and magnetite was also elucidated.

2. Materials and methods

2.1. Materials

Magnetite, Carboxyl-modified polystyrene nanoplastics (COOH-PSNPs, 2.5 % w/v), and HA were purchased from Shanghai Aladdin Biochemical Technology Co., Ltd. SA and BSA were purchased from Sangon Biotech (Shanghai) Co., Ltd. Other chemicals were purchased from Shanghai Chemical Reagent Corporation, China. All reagents were of analytical reagent grade.

The magnetite sample used in this experiment was confirmed to be pure magnetite by XRD pattern (Fig. S1). The specific surface area of magnetite was measured to be $14.124 \text{ m}^2/\text{g}$ using a nitrogen adsorption apparatus. The sample of COOH-PSNPs received was a 300 nm suspension containing 2.5 % w/v COOH-PSNPs. 125 ppm COOH-PSNPs suspension was prepared by diluting 5 mL COOH-PSNPs stock solution in 1 L of ultrapure water for subsequent experiments. Fig. S2 confirms that COOH-PSNPs used in this study were uniform particles with a diameter of 300 nm. HA, SA, and BSA were dissolved in ultrapure water to prepare 100 ppm solution, and stored in a refrigerator at 4°C for subsequent experiments. Ultrapure water was used in all experiments in this study.

2.2. Characterization

The morphologies of COOH-PSNPs, magnetite, and the solid specimens of suspension containing COOH-PSNPs and magnetite after interaction for 5 h under different conditions, were examined by scanning electron microscope (SEM, Scios, FEI Company) and transmission electron microscope (TEM, G2 F20 S-TWIN, Tecnai). High-sensitivity zeta potential analyzer (Omni, Brookhaven) was used to measure the zeta potentials of COOH-PSNPs and magnetite at pH 3.0, 6.5, and 10.0. In order to better explain the interaction mechanisms between COOH-PSNPs and magnetite under various conditions, attenuated total reflectance-Fourier transform infrared spectroscopy (ATR-FTIR, Vertex 70 spectrometer, BRUKER optics) was used to analyze the types of surface groups of samples before and after the reaction. The phase structure of the magnetite sample was characterized by X-ray diffraction (XRD, Empyrean, PANalytical B.V) operating with Cu-K α radiation. The specific surface area was analyzed by a multi-point BET method using a nitrogen adsorption apparatus (Autosorb-iQ2-MP, Quantachrome, Boynton Beach, FL, USA).

2.3. Deposition experiments of COOH-PSNPs with magnetite

The deposition experiments of COOH-PSNPs with magnetite were carried out in 250 mL conical flasks. All experiments in this study were performed at an initial COOH-PSNPs concentration of 20 ppm, which was a commonly used concentration of COOH-PSNPs in prior studies (Nie et al., 2023; Xie et al., 2023; Lin et al., 2024; Wang et al., 2023b). In a typical experiment, the initial pH of COOH-PSNPs solution was adjusted by adding HCl or NaOH. 50 mL COOH-PSNPs solution (40 ppm) and 50 mL water containing 0.01 g magnetite were firstly adjusted to the requisite initial pH, and then mixed together for further deposition experiments. Except for the study of pH effect, the deposition experiments were carried out at initial pH 6.5. The mixtures containing COOH-PSNPs and magnetite were agitated at room temperature (except for the study of temperature effect) and 200 rpm in an orbital incubator shaker (ZWYR-D2403, Zhicheng) to ensure a uniform interaction between COOH-PSNPs and magnetite. 10 mL of the suspension was sampled at different time intervals (0, 10, 30, 60, 90, 120, 150, 180, 240, and 300 min), and magnetite was separated magnetically from the suspension and the supernatant was carefully collected. After that, the

absorbance of COOH-PSNPs in supernatant was measured by ultraviolet-visible spectrophotometer (UV-VIS, Cary 300, Agilent) at a wavelength of 234 nm (Nie et al., 2023; Xie et al., 2023; Lin et al., 2024). The deposition extent of COOH-PSNPs was calculated by the ratio of the COOH-PSNP suspended concentration (C) and the initial COOH-PSNP concentration (C_0) at different times. The relationship between C/C_0 and time (t) was used to plot the normalized deposition curves.

In order to better simulate the natural water environment, the effects of ionic type and OMs were also studied. Ions such as KCl, NaCl, $MgCl_2$, $CaCl_2$, NaF, $NaNO_3$, Na_2SO_4 , Na_2CO_3 , and NaH_2PO_4 are common in natural water environment (Xie et al., 2023). Cr(VI) is a common and highly toxic heavy metal in the environment, and magnetite has a good adsorption capacity for Cr(VI) (Yuan et al., 2010), which may have a significant effect on the heteroaggregation deposition of COOH-PSNPs with magnetite. Consequently, the effect of $K_2Cr_2O_7$ was included in the study. The HA, SA, and BSA (as substitutes for humus, polysaccharide, and protein, respectively) were selected respectively, which were the representative OMs commonly used in previous experiments (Xie et al., 2023; Duan et al., 2021; Liu et al., 2020; Wu et al., 2021). Therefore, in this study, the effects of initial pH (3.0, 5.0, 6.5, 8.0, and 10.0), temperature (15, 25, 35, 45, and 55 °C), ionic type (cations: KCl, NaCl, $MgCl_2$, and $CaCl_2$; anions: NaF, NaCl, $NaNO_3$, Na_2SO_4 , Na_2CO_3 , NaH_2PO_4 , and $K_2Cr_2O_7$), and the concentration was set to 5 mM), phosphate concentration (0–10 mM), and OMs (HA, SA, and BSA) on the deposition behaviors of COOH-PSNPs with magnetite were determined. Wherein the concentration range of OMs was 0–10 ppm. When OMs existed, magnetite was firstly added to the solution containing OMs for shaking 2 h, then COOH-PSNPs solution was added to react with them. In order to verify the role of hydrogen bond and hydrophobic interaction in the deposition of COOH-PSNPs, 5 mM urea (a hydrogen bond breaker) and 50 % dimethyl sulfoxide (DMSO, a dipolar aprotic organic solvent) were added to the solution, respectively (Xie et al., 2023). In order to further explain the heteroaggregation mechanism of COOH-PSNPs and magnetite, deaggregation experiments were carried out. Deaggregation experiments are presented in the Supplementary Material. Each experimental data was the average of the data from two parallel experiments. The solid specimens separated magnetically from the suspension were dried at 30 °C, and their morphologies and chemical surface groups were characterized using SEM, TEM, and ATR-FTIR.

3. Results and discussion

3.1. Effects of solution chemistry on deposition of COOH-PSNPs with magnetite

3.1.1. Effects of pH and temperature

As shown in Fig. 1a, pH had a significant effect on the deposition of COOH-PSNPs with magnetite. About 100 % of COOH-PSNPs were deposited within 2.5 h when the pH was between 3.0 and 6.5. SEM

images (Fig. 2a) showed the formation of COOH-PSNPs-magnetite heteroaggregates, and the number of heteroaggregates was consistent with the deposition curves of COOH-PSNPs, indicating that the heteroaggregation of COOH-PSNPs with magnetite was the main factor leading to the deposition of COOH-PSNPs. With increasing pH from 6.5 to 8.0, the deposition rates of COOH-PSNPs decreased significantly. No deposition of COOH-PSNPs occurred and no COOH-PSNPs-magnetite heteroaggregates could be observed within 5 h at pH 8.0 or 10.0. The zeta potentials of COOH-PSNPs and magnetite at different pHs are presented in Fig. S3a. COOH-PSNPs exhibited a highly negative charge at pH 3.0–10.0. This was attributed to the presence of a large number of negatively charged carboxyl groups ($-COO^-$) on the surface of COOH-PSNPs (Nie et al., 2023; Xie et al., 2023). The pH_{IEP} (isoelectric point) of magnetite was at about pH 6.8 (Liang et al., 2021). When $pH < 6.8$, with the increase of pH, the protonation on the surface of magnetite decreased, and the positive charge on the surface of magnetite gradually decreased, which leads to the decrease of electrostatic attraction between COOH-PSNPs and magnetite. Therefore, the deposition rates of COOH-PSNPs with magnetite decreased with the increase of pH. For example, when the pH was 3.0, 5.0, or 6.5, the deposition rates of COOH-PSNPs with magnetite at 10 min were 36 %, 30 %, and 19 %, respectively. When $pH > 6.8$, the surface charge of magnetite was reversed to negative charge due to the deprotonation of magnetite. The negative charge of magnetite increased with the increase of pH, so the electrostatic repulsion between magnetite and negatively charged COOH-PSNPs increased, thus hindering the deposition of COOH-PSNPs with magnetite. When pH was 8.0 or 10.0, the deposition rates of COOH-PSNPs decreased to nearly zero after interaction with magnetite for 5 h.

In order to verify the deposition mechanism of COOH-PSNPs with magnetite, 5 M urea and 50 % DMSO were added to verify the role of hydrogen bonding and hydrophobic interaction in the deposition of COOH-PSNPs. Fig. 1b showed the deposition profiles of COOH-PSNPs with magnetite at pH 6.5 in the presence of 5 M urea and 50 % DMSO. The deposition of COOH-PSNPs was significantly inhibited by 5 M urea, and only about 8 % of COOH-PSNPs were deposited within 5 h, suggesting that hydrogen bond should be the predominant force between COOH-PSNPs and magnetite (Zandieh and Liu, 2022). 50 % DMSO had no significant effect on the deposition of COOH-PSNPs with magnetite, and COOH-PSNPs were almost completely deposited within 2.5 h, indicating that hydrophobic interaction played negligible role in the deposition of COOH-PSNPs. ATR-FTIR spectra of magnetite before and after mixing with COOH-PSNPs were systematically investigated (Fig. S4). The stretching vibration peak of Fe–O bond of magnetite was observed at 544 cm^{-1} (Lee and Kim, 2022). For COOH-PSNPs, the peaks at 698, 758, 1452, 1492, 1601, 2922, and 3026 cm^{-1} were the characteristic peaks of polystyrene (Huang et al., 2022). The peaks at 540 and 1197 cm^{-1} were ascribed to the C–H vibration, and the peak at 1726 cm^{-1} was ascribed to the stretching vibration of carboxyl in

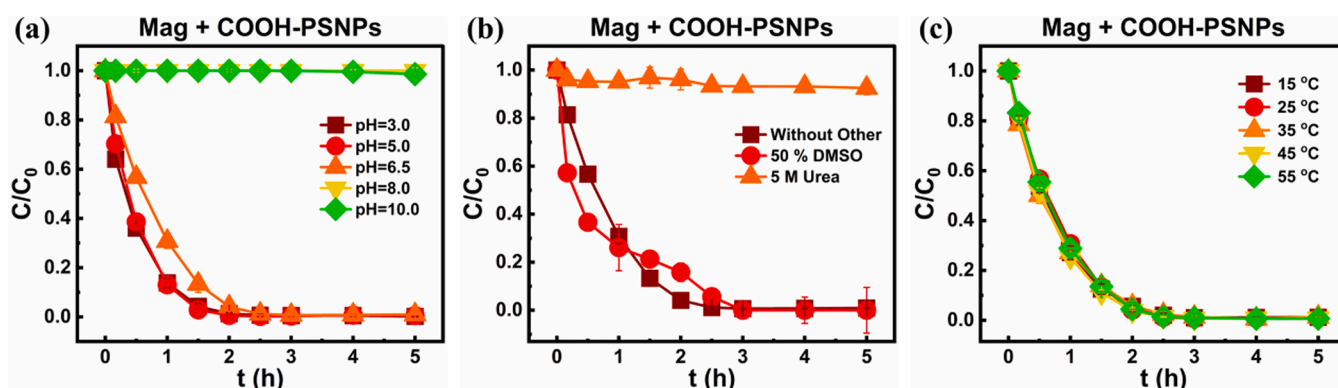


Fig. 1. Deposition profiles of COOH-PSNPs with magnetite: (a) at different pHs; (b) in the presence of urea and DMSO and (c) at different temperatures at pH 6.5.

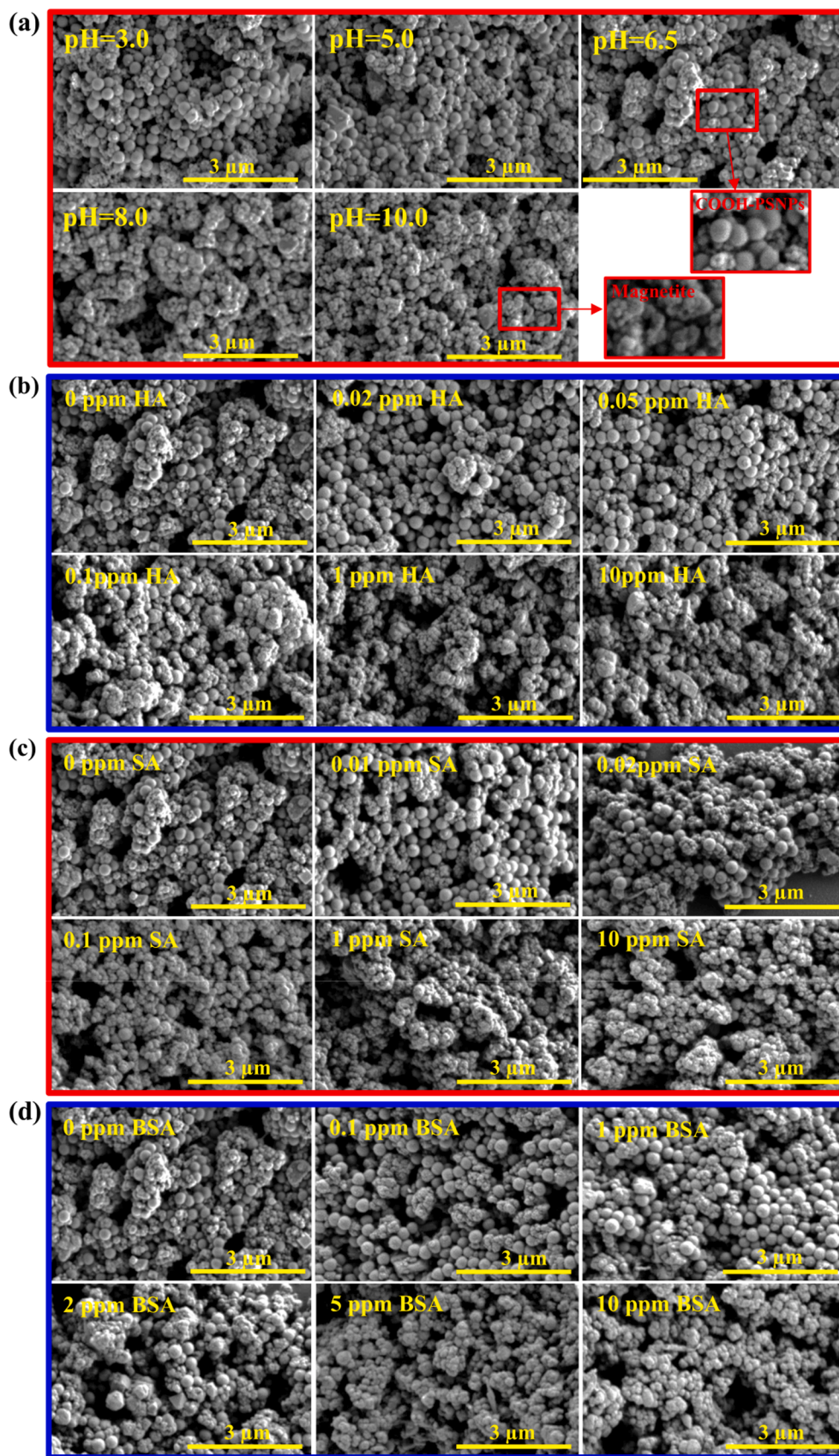


Fig. 2. SEM images of magnetite after interaction with COOH-PSNPs for 5 h under different conditions: (a) different pHs; different concentrations of (b) HA, (c) SA, and (d) BSA at pH 6.5.

COOH-PSNPs (Xie et al., 2023; Wang et al., 2023a). At pH 3.0–6.5, COOH-PSNPs were deposited by magnetite, and the typical peaks of COOH-PSNPs could be observed on magnetite. At pH 8.0 and 10.0, the characteristic peaks of COOH-PSNPs could not be observed on magnetite, which further confirms that COOH-PSNPs could not heteroaggregate with magnetite at these pHs. At pH 3.0 and 6.5, the peak position of Fe–O bond for magnetite shifted from 544 to 549 and 555 cm^{-1} after the interaction between COOH-PSNPs and magnetite, indicating that the Fe–O bond of magnetite may have formed hydrogen bonds with –CH, –OH, and –COOH on the surface of COOH-PSNPs. In addition, negatively charged substances can form complexes with proton-containing and positively charged substances through charge-assisted hydrogen bonding (CAHB) or electrostatic forces (Song et al., 2024). The bond energy of CAHB is four times that of normal hydrogen bonds due to electrostatic attraction, making CAHB possess a certain degree of covalent character (Mahmudov et al., 2017; Li et al., 2023). Magnetite belongs to hydrophilic minerals (Zandieh and Liu, 2022; Rhein et al., 2022), and it will be positively charged by the presence of a small amount of protonated hydroxyl groups ($-\text{OH}_2^+$) on the surface at pH 6.5 ($\text{pH} < \text{pH}_{\text{IEP}}$), which may create charge-assisted hydrogen bonding with the negatively charged COOH-PSNPs. Therefore, hydrogen bonds (i.e., $-\text{C}-\text{O}\cdots\text{H}-\text{O}-\text{Fe}$, $-\text{C}-\text{H}\cdots\text{O}-\text{Fe}$, and $-\text{C}-\text{O}-\text{H}\cdots\text{O}-\text{Fe}$), CAHB, and electrostatic interactions dominated the deposition behavior of COOH-PSNPs depending on the solution pH. In the deaggregation experiments by changing pH, no deaggregation occurred when pH was 3.0, 5.0, 6.5, or 8.0, and only about 18 % of COOH-PSNPs deaggregated when pH was 10.0 (Fig. S5). It may be due to hydrogen bonds and strong CAHB generated during heteroaggregation of COOH-PSNPs with magnetite that hindered the deaggregation of COOH-PSNPs. Therefore, the deaggregation experiments further confirmed the possibility of hydrogen bonding and CAHB between COOH-PSNPs and magnetite in addition to electrostatic interaction.

Fig. 1c shows the effect of temperature on the deposition of COOH-PSNPs. As the temperature of the solution increased from 15 to 55 °C, the deposition curves of COOH-PSNPs with magnetite almost overlapped. With the increase of temperature, the stability of hydrogen bonds decreases (Ross and Rekharsky, 1996), and the absolute value of zeta potentials of magnetite and COOH-PSNPs significantly decreased (Fig. S3b), leading to the reduction of COOH-PSNPs heteroaggregation rates. However, higher temperature was favorable for Brownian motion and led to quicker aggregation of PSNPs (Ling et al., 2022). Therefore, temperature had negligible effect on the deposition of COOH-PSNPs with magnetite.

3.1.2. Effect of ionic type

As shown in Fig. 3a and b, COOH-PSNPs were completely deposited within 2.5 h in the absence of ions at pH 6.5. The addition of KCl, NaCl, MgCl_2 , CaCl_2 , NaF, NaNO_3 , Na_2SO_4 , or Na_2CO_3 had insignificant effect

on the heteroaggregation of COOH-PSNPs with magnetite. However, the addition of NaH_2PO_4 or $\text{K}_2\text{Cr}_2\text{O}_7$ significantly inhibited the deposition of COOH-PSNPs, and negligible deposition of COOH-PSNPs after 5 h was observed.

At pH 6.5, cations had a negligible effect on the zeta potential of magnetite (Fig. S6a). The monovalent cations had an insignificant effect on the surface charge of COOH-PSNPs, while divalent cations (Ca^{2+} and Mg^{2+}) caused a significant decrease in the zeta potentials of COOH-PSNPs from -58.30 mV to -36.99 mV and -35.33 mV, respectively (Fig. S6b). This can be attributed to the fact that divalent cations exhibited stronger ability to neutralize surface negative charges and compress the electric double layer than univalent cations (Kong et al., 2023; Li et al., 2021b), and had the same ability to neutralize surface negative charges by cations with the same valence state (Xie et al., 2023). The negative surface charge of COOH-PSNPs was decreased, resulting in a lower electrostatic attraction between COOH-PSNPs and magnetite. However, the deposition rates of COOH-PSNPs remained unaltered, which further confirms that electrostatic force was not the dominant force of heteroaggregations between COOH-PSNPs and magnetite. The influence of anions on COOH-PSNPs deposition may be related to zeta potentials. With the addition of NaH_2PO_4 or $\text{K}_2\text{Cr}_2\text{O}_7$, the zeta potentials of magnetite changed from positive (3.28 mV) to negative (-39.97 mV and -27.96 mV) (Fig. 4a). COOH-PSNPs carried highly negative charge (between -56.01 mV and -76.91 mV) regardless of the presence or absence of anions (Fig. 4b). H_2PO_4^- could form inner-sphere surface complexes with magnetite (Liang et al., 2021; Lin et al., 2023), and $\text{Cr}_2\text{O}_7^{2-}$ could be adsorbed and immobilized on magnetite surface through redox and isomorphic substitution (Yuan et al., 2010; Zhang et al., 2017a), effectively neutralizing the surface charge and even reversing the surface charge of magnetite from positive to negative, leading to strong repulsive electrostatic forces and high energy barriers between negatively charged magnetite and COOH-PSNPs. Therefore, the occurrence of competitive adsorption between COOH-PSNPs and H_2PO_4^- or $\text{Cr}_2\text{O}_7^{2-}$ on the surface of magnetite and electrostatic repulsion inhibited the deposition of COOH-PSNPs with magnetite. When NaCl, NaNO_3 , Na_2SO_4 , or Na_2CO_3 was present, there were negligible effects on the zeta potentials of magnetite and COOH-PSNPs (Fig. 4a and b), and therefore no effects on the deposition of COOH-PSNPs with magnetite. The zeta potential of magnetite in the presence of NaF was -5.32 mV (Fig. 4a). It could be ascribed that F^- can be adsorbed on the surface of magnetite by replacing $-\text{OH}$ and protonated $-\text{OH}_2^+$ (Zhang et al., 2017b; Xu et al., 2007), leading to the change of surface charge of magnetite. Fluorine (F) adsorbed on the magnetite surface can also form hydrogen bonds with $-\text{C}-\text{H}$, $-\text{OH}$, and $-\text{COOH}$ of COOH-PSNPs (Manna et al., 2015; Dalvit and Vulpetti, 2016). F atom is known to have smaller atomic radius and greater electronegativity than oxygen (O) atom, thus it can form stronger hydrogen bonds with $-\text{C}-\text{H}$, $-\text{OH}$, or $-\text{COOH}$. Furthermore, F^- could change the electrification of magnetite, resulting

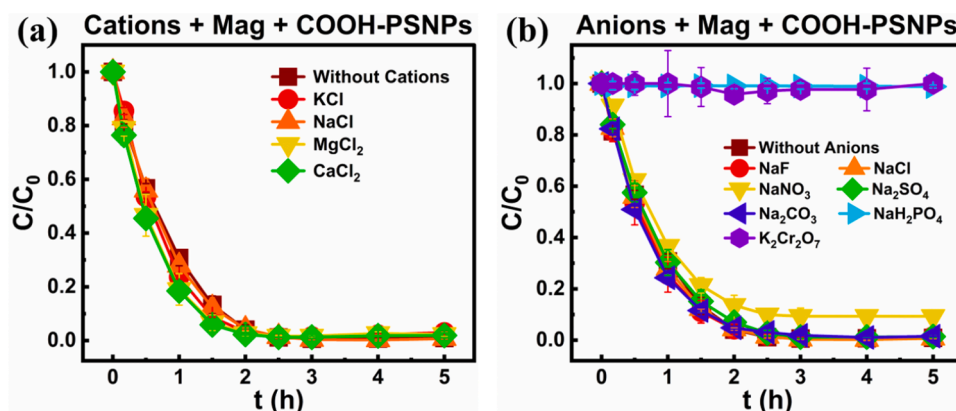


Fig. 3. Deposition profiles of COOH-PSNPs with magnetite in the presence of (a) different cations and (b) different anions at pH 6.5.

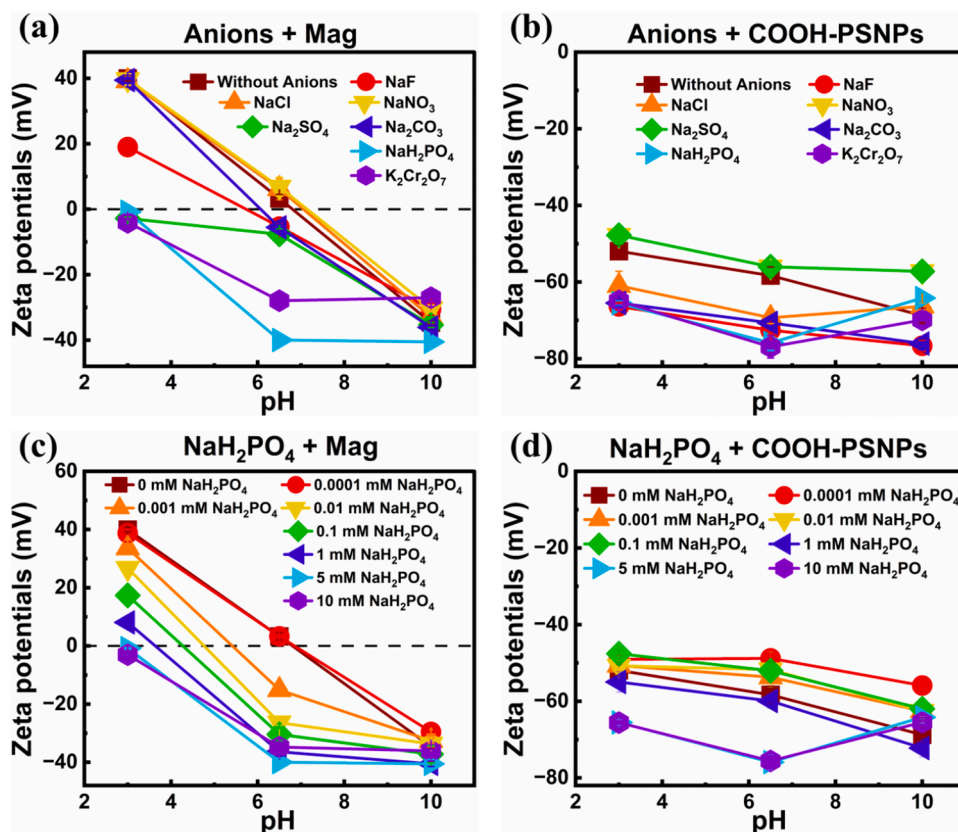


Fig. 4. Zeta potentials of magnetite (a, c) and COOH-PSNPs (b, d) in the presence of 5 mM various anions and different concentrations of phosphate at different pH values.

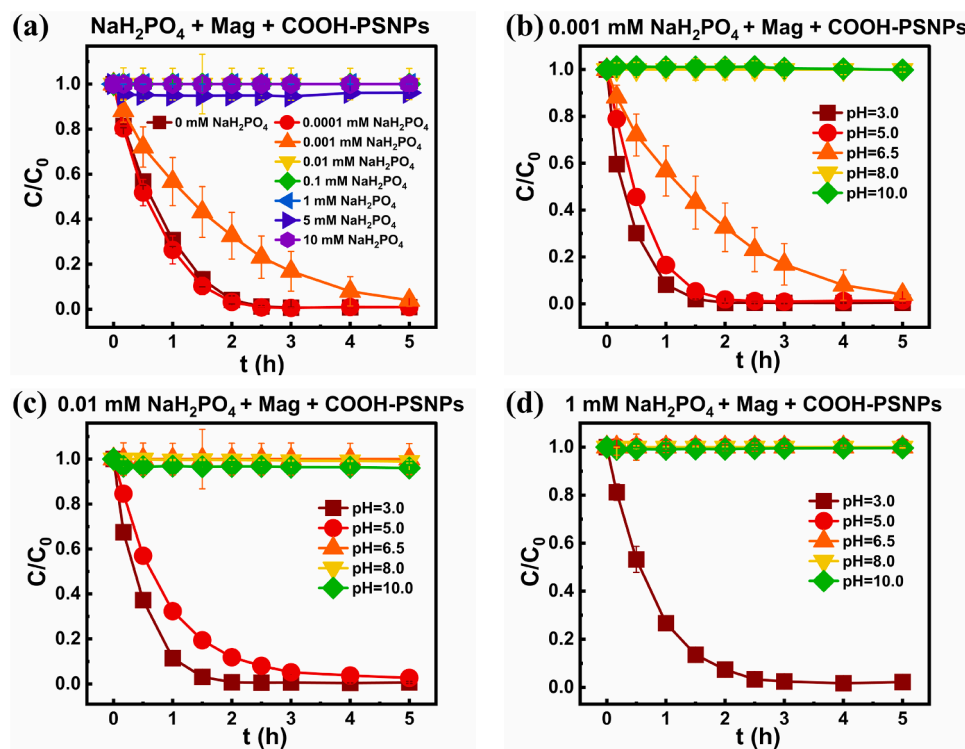


Fig. 5. Deposition profiles of COOH-PSNPs with magnetite: (a) different phosphate concentrations at pH 6.5; at different pHs (b) 0.001 mM phosphate, (c) 0.01 mM phosphate, and (d) 1 mM phosphate.

in electrostatic repulsion between magnetite and COOH-PSNPs. Therefore, the combined effects of increased electrostatic repulsion and hydrogen bond force determined the negligible deposition of COOH-PSNPs with magnetite.

3.1.3. Effect of phosphate

Phosphorus (P) is an essential nutrient for aquatic biota, but eutrophication of freshwater in lakes, rivers, and oceans is a serious global environmental problem (Lin et al., 2023; Lee and Kim, 2017; Hou et al., 2020). The presence of phosphate will alter the surface physicochemical properties of iron (hydr)oxides minerals and affect the interaction between minerals and NPs (Amstaeffer et al., 2012; Hiemstra, 2018). Iron (hydr)oxides have high adsorption affinity toward phosphate (Liang et al., 2021). It was speculated that phosphate might significantly affect the interfacial interaction between COOH-PSNPs and magnetite. Therefore, the effect of phosphate on the deposition of COOH-PSNPs with magnetite was further investigated. As shown in Fig. 5a, low concentrations of phosphate could significantly inhibit the deposition of COOH-PSNPs at pH 6.5. As phosphate concentration increased from 0 to 0.01 mM, the deposition rates of COOH-PSNPs decreased from 100 % to 0 %. When the concentration of phosphate exceeded 0.01 mM, the deposition of COOH-PSNPs with magnetite was completely inhibited. This was also correlated with the change in their zeta potentials (Fig. 4c and d). Low concentrations of phosphate significantly reduced the zeta potentials of magnetite, e.g., the zeta potentials of magnetite were 3.28, 3.27, -15.12, and -26.35 mV at pH 6.5 in the presence of 0, 0.0001, 0.001, or 0.01 mM phosphate, respectively. At pH 6.5, phosphate existed in solution mainly in the form of H_2PO_4^- and HPO_4^{2-} (Lee and Kim, 2022), and the negatively charged phosphate could be specifically adsorbed on the surface of the magnetite via inner-sphere complexation, ion exchange and electrostatic attraction. The primary mechanism is the inner-sphere complexation between Fe and phosphate (Lee and Kim, 2022; Lin et al., 2023), reversing the surface charge of the magnetite from positive to negative. Similarly, Xie et al. found that the specific adsorption of phosphate on goethite could penetrate the electric double layer more easily than other ions, effectively neutralizing the surface charge, leading to the surface potential reversal of goethite from positive to negative, thus significantly inhibiting the deposition of COOH-PSNPs with goethite due to enhanced electrostatic repulsion (Xie et al., 2023).

Fig. 5b, c, and d represent the deposition curves of COOH-PSNPs with magnetite at 0.001, 0.01, and 1 mM phosphate concentration at different pHs, respectively. As shown, the deposition of COOH-PSNPs with magnetite was highly dependent on pH at all phosphate concentrations, and the deposition extent of COOH-PSNPs showed a significant negative correlation with pH and phosphate concentration. Both pH (3.0–10.0) and the concentrations of phosphate (0–10 mM) had negligible effects on the surface potential of COOH-PSNPs, but they showed significant effects on the zeta potential of magnetite (Fig. 4c and d). In the presence of low phosphate concentration (0.001 mM) (Fig. 5b), the deposition rates of COOH-PSNPs decreased gradually with increasing pH. The deposition extent of COOH-PSNPs was 100 %, 99 %, and 77 % at pH 3.0, 5.0, and 6.5 within 2.5 h, respectively, and was 100 % at pH 6.5 within 5 h. The deposition extent of COOH-PSNPs was 0 % within 5 h at pH 8.0 and 10.0. The deposition of COOH-PSNPs was significantly correlated with the zeta potential of magnetite. Although both magnetite and COOH-PSNPs were negatively charged at pH 6.5 and electrostatic repulsion prevented their heteroaggregation, the strong hydrogen bond that existed between them could overcome the energetic barrier of repulsion, leading to the reduced deposition rates of COOH-PSNPs with magnetite. When the pH was 8.0 or 10.0, the surface charges of magnetite were more negative, generating larger electrostatic repulsion and energy barriers to COOH-PSNPs, preventing their heteroaggregation and stabilizing the COOH-PSNPs in suspension. Similar trends were observed for the deposition of COOH-PSNPs in the presence of 0.01 or 1 mM phosphate. No deposition of COOH-PSNPs with magnetite occurred when the pH was above 6.5 and 5.0 with addition of 0.01 and

1 mM phosphate, respectively. These results indicated that the electrostatic repulsion between COOH-PSNPs and magnetite originated from the specific adsorption of phosphate on magnetite inhibited the deposition of COOH-PSNPs in the presence of phosphate.

3.2. Effects of organic macromolecules on the deposition of COOH-PSNPs with magnetite

3.2.1. Deposition profiles of COOH-PSNPs with magnetite in the presence of organic macromolecules

Interactions between mineral and OMs to form mineral-OM associations through electrostatic interactions, hydrogen bonds, and ligand exchange, are commonly existed in a variety of natural environments, which will alter the original physicochemical properties of mineral surfaces and play crucial roles in regulating the deposition of NPs with minerals (Bao et al., 2021; Zhou et al., 2014; Lee and Hur, 2020; Safiur Rahman et al., 2013). OMs and minerals existed earlier in natural water bodies than artificial NPs (Kong et al., 2023). Therefore, in order to investigate the deposition behaviors of COOH-PSNPs with minerals in the presence of OMs, magnetite and a series of concentrations of OMs (HA, SA, and BSA) were first mixed in solution for 2 h to form magnetite-OM associations, and then COOH-PSNPs were added for further deposition experiments.

As shown in Fig. 6, three OMs significantly inhibited the deposition of COOH-PSNPs with magnetite, and the inhibition effect enhanced with the increase of the concentration of OMs. Specifically, the deposition of COOH-PSNPs decreased significantly as HA concentration increased from 0 to 0.2 ppm (Fig. 6a). In the presence of 0, 0.1, and 0.2 ppm HA, about 100 %, 27 %, and 0 % of COOH-PSNPs were deposited within 5 h, respectively. Increasing SA concentration from 0 to 0.1 ppm markedly decreased the deposition rates of COOH-PSNPs. When SA concentration exceeded 0.1 ppm, almost no deposition of COOH-PSNPs was observed within 5 h (Fig. 6b). As BSA concentration increased from 0 to 5 ppm, the deposition rates of COOH-PSNPs also remarkably decreased (Fig. 6c). Overall, the inhibition capacities of the three OMs followed an order of SA > HA > BSA, and the minimum inhibitory concentrations of SA, HA, and BSA for the deposition of COOH-PSNPs were 0.1, 0.2, and 5 ppm, respectively.

SEM images of magnetite after mixing COOH-PSNPs for 5 h under different OMs with a series of concentrations are shown in Fig. 2b, c, and d. It can be visually observed that the number of COOH-PSNPs-magnetite heteroaggregates remarkably decreased with increasing the concentration of OMs. The COOH-PSNPs-magnetite heteroaggregates could not be observed when the concentration of HA, SA, and BSA exceeded 0.2, 0.1, and 5 ppm, respectively, confirming that OMs could significantly inhibit the deposition of COOH-PSNPs with magnetite.

3.2.2. Interfacial interaction mechanisms between COOH-PSNPs and magnetite in the presence of organic macromolecules

In order to further clarify the influence of OMs on the deposition of COOH-PSNPs with magnetite, zeta potentials, ATR-FTIR spectroscopy, and TEM were used to analyze the interfacial interaction mechanisms between COOH-PSNPs and magnetite in the presence of OMs. Fig. S7 shows the zeta potentials of COOH-PSNPs and magnetite in the presence and absence of OMs. At pH 6.5, the zeta potentials of HA, SA, and BSA were -49.18, -39.23, and -24.24 mV, respectively. The zeta potentials of COOH-PSNPs were highly negative (-42.82 ~ -61.64 mV) regardless of the presence or absence of OMs (Fig. S7a, c, and e). The decrease in zeta potentials of magnetite after reacting with three OMs indicates that the OMs were adsorbed on the surface of the magnetite (Fig. S7b, d, and f). The electrostatic attraction between positively charged magnetite and negatively charged OMs facilitated the adsorption of OMs onto the surface of magnetite, thus neutralizing the surface charge of magnetite. The increase in the concentration of OMs induced more OMs to adsorb onto the surface of magnetite, resulting in the charge reversal of magnetite. The deposition of COOH-PSNPs in the presence of OMs

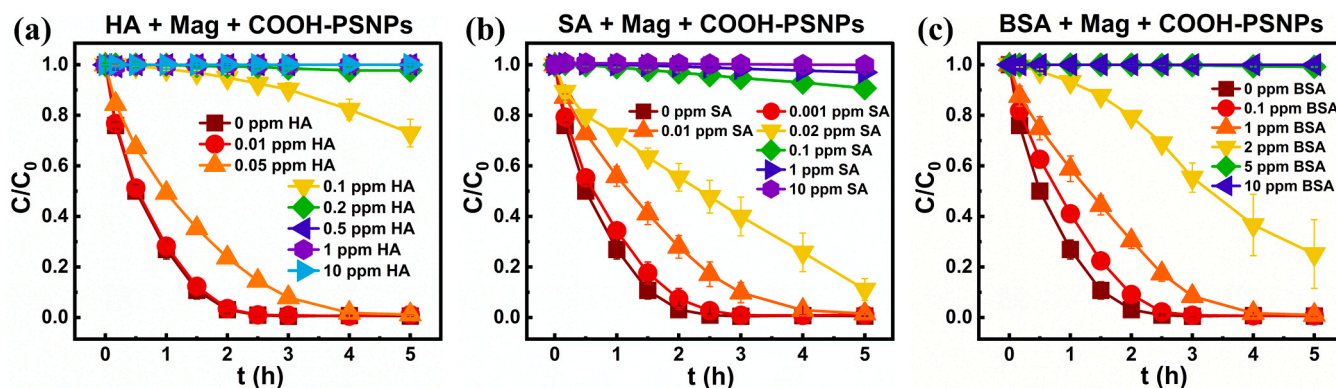


Fig. 6. Deposition profiles of COOH-PSNPs with magnetite at pH 6.5 in the presence of different concentrations of (a) HA, (b) SA, and (c) BSA.

was correlated with the zeta potentials of magnetite, and the deposition rates of COOH-PSNPs decreased with the increase in the negative charge on magnetite surface (Fig. 6; Fig. S7b, d, and f). The reversal degree of the surface charge of magnetite in the presence of HA, SA, and BSA was consistent with their inhibition capacities for the deposition of COOH-PSNPs, and thus electrostatic repulsion should be the main mechanism for inhibiting the deposition of COOH-PSNPs in the presence of HA, SA, and BSA.

The ATR-FTIR spectra of magnetite in the presence and absence of OMs are shown in Fig. S8a, b, and c. The absorption peaks of organics could be observed on magnetite in the presence of OMs, and the peak intensities were positively correlated with the concentration of OMs. For HA and SA, the peaks at 1031 and 1024 cm^{-1} were attributed to the C–O stretching vibration, and the broad adsorption peaks at about 3300 cm^{-1} were attributed to the stretching vibration of –OH. The peaks at 1363, 1404, and 1544 cm^{-1} , and 1591 cm^{-1} respectively represented the C=O symmetric and asymmetric stretching of the carboxyl group (Xie et al., 2023). For BSA, the peak at about 1389 cm^{-1} belonged to C–O and N–H bending vibration and C–N stretching. The peak at 1528 cm^{-1} was ascribed to C–N stretching vibration and N–H bending vibration. The peak at 1637 cm^{-1} belonged to C=O and N–H stretching vibration. The peak at 3285 cm^{-1} corresponded to N–H stretching vibration of amino group (Wu et al., 2021). After interaction with magnetite, the adsorption peaks of OMs could be observed, suggesting that HA, SA, and BSA could be adsorbed on the magnetite surface (Safur Rahman et al., 2013). In addition, ATR-FTIR spectra of magnetite before and after mixing with COOH-PSNPs in the absence and presence of HA (Fig. S8d), SA (Fig. S8e), and BSA (Fig. S8f) were analyzed. The characteristic absorption peaks of COOH-PSNPs were observed on magnetite after mixing with COOH-PSNPs, and the peak intensity was negatively correlated with the concentration of OMs. The characteristic absorption peaks of COOH-PSNPs could not be observed when the concentrations of HA, SA, and BSA were greater than 0.2, 0.1, and 5 ppm, respectively. This result further confirmed that OMs could react with the surface of magnetite, thus hindering the heteroaggregation and deposition of COOH-PSNPs with magnetite.

OMs could interact with COOH-PSNPs (Xie et al., 2023; Li et al., 2021b; Saavedra et al., 2019) and magnetite (Zhou et al., 2015; Hu et al., 2010; Li et al., 2018) to form layers of organic matter on their surfaces, which could inhibit the deposition of COOH-PSNPs with magnetite through the steric hindrance effect of the organic matter layers. As shown in the TEM image (Fig. S9), the COOH-PSNPs-magnetite heteroaggregates were observed when OMs were not present. In the presence of 10 ppm OMs, no heteroaggregate could be observed, confirming that the deposition of COOH-PSNPs was completely inhibited under this OMs concentration. In addition, organic macromolecular layers encapsulated on the surface of magnetite and COOH-PSNPs were clearly observed (Fig. S9), suggesting that OMs could induce great steric hindrance to inhibit the heteroaggregation and deposition of COOH-PSNPs with

magnetite.

In addition, the three OMs had different abilities to inhibit the heteroaggregation and deposition of COOH-PSNPs with magnetite. In this experiment, the lowest concentrations of HA, SA, and BSA that completely inhibited the deposition of COOH-PSNPs were 0.2, 0.1, and 5 ppm, respectively. It is postulated that this phenomenon may be closely related to their charge density, hydrophilicity, and structure. The order of hydrophilicity of the three OMs is SA > HA > BSA (Liu et al., 2020), which is consistent with their inhibition ability to the deposition of COOH-PSNPs. COOH-PSNPs and magnetite are hydrophilic substances (Zandieh and Liu, 2022; Rhein et al., 2022), and therefore, it can be postulated that SA is more likely to adsorb on the surfaces of COOH-PSNPs and magnetite than HA and BSA. Moreover, in terms of the structure of organic macromolecules, SA is a linear and semi-flexible macromolecule, HA is a globular and semi-rigid macromolecule, and BSA is a globular macromolecule with the tertiary structure of protein (Xie et al., 2023; Liu et al., 2020). The linear and flexible structure of SA showed strong ductility and will be easily adhered to the surface of particles to produce higher steric hindrance as compared with HA and BSA (Huang et al., 2022; Xie et al., 2023). Due to the hydrophilicity, linear and flexible structure, and high surface charge density of SA, it will be more easily adsorbed onto the surfaces of COOH-PSNPs and magnetite, changing the chargeability of magnetite surface and generating steric hindrance effect. The absolute values of zeta potentials of the three OMs followed the order of HA (–49.18 mV) > SA (39.23 mV) > BSA (–24.24 mV). However, when the concentrations of HA and SA were 0.2 and 0.1 mM, the zeta potentials of magnetite were –30.75 and –31.75 mV, respectively, implying that SA was more easily attached to magnetite surface. Thus, based on above discussion, it could be concluded that the enhanced steric hindrance and electrostatic interactions between COOH-PSNPs and magnetite-OM associations in the presence of OMs could inhibit the interfacial interaction and deposition of COOH-PSNPs with magnetite.

4. Conclusion

The results indicated that COOH-PSNPs could heteroaggregate with magnetite by electrostatic attraction, hydrogen bond, and CAHB. The deposition rates of COOH-PSNPs with magnetite decreased with increasing solution pH. The effect of temperature on COOH-PSNPs deposition was negligible. Cations exerted a negligible effect on the heteroaggregation of COOH-PSNPs with magnetite, whereas anions such as phosphate and dichromate significantly inhibited the deposition of COOH-PSNPs through competitive adsorption and electrostatic repulsion. Moreover, the low concentration of phosphate could effectively reverse the surface charge of magnetite and significantly inhibit the deposition of COOH-PSNPs. OMs significantly inhibited the interfacial interaction and deposition of COOH-PSNPs with magnetite by enhancing the electrostatic repulsion and steric hindrance between

COOH-PSNPs and magnetite due to the formation of magnetite-OM associations. Meanwhile, the ability of OMs for inhibiting the deposition of COOH-PSNPs followed the sequence of SA > HA > BSA. These findings may provide new insights into a deeper understanding of geochemistry behaviors of COOH-PSNPs associated with magnetite and organic matter in natural environments. Moreover, our results also show the potential that magnetite may be used as a good candidate for effectively removing nanoplastics from the natural aquatic environment.

CRedit authorship contribution statement

Meimei Ran: Writing – original draft, Validation, Investigation, Formal analysis. **Xin Nie:** Writing – review & editing, Supervision, Resources, Project administration. **Jingxin Wang:** Supervision, Formal analysis. **Ruiyin Xie:** Methodology, Formal analysis. **Xiaoping Lin:** Methodology, Formal analysis. **Hanjun Zhu:** Methodology. **Quan Wan:** Supervision, Project administration. **Yuhong Fu:** Writing – review & editing, Supervision, Methodology, Funding acquisition, Conceptualization.

Declaration of Competing Interest

The authors declare that they have no known competing financial interests or personal relationships that could have appeared to influence the work reported in this paper.

Acknowledgments

This work was financially supported by National Natural Science Foundation of China (No. 42162006).

Appendix A. Supporting information

Supplementary data associated with this article can be found in the online version at [doi:10.1016/j.ecoenv.2024.117608](https://doi.org/10.1016/j.ecoenv.2024.117608).

Data Availability

Data will be made available on request.

References

- Amstaetter, K., Borch, T., Kappler, A., 2012. Influence of humic acid imposed changes of ferrihydrite aggregation on microbial Fe(III) reduction. *Geochim. Cosmochim. Acta* 85, 326–341. <https://doi.org/10.1016/j.gca.2012.02.003>.
- Bao, Y., Bolan, N.S., Lai, J., Wang, Y., Jin, X., Kirkham, M.B., Wu, X., Fang, Z., Zhang, Y., Wang, H., 2021. Interactions between organic matter and Fe (hydro)oxides and their influences on immobilization and remobilization of metal(loid)s: a review. *Crit. Rev. Environ. Sci. Technol.* 52 (22), 4016–4037. <https://doi.org/10.1080/10643389.2021.1974766>.
- Bellingeri, A., Casabianca, S., Capellacci, S., Faleri, C., Paccagnini, E., Lupetti, P., Koelmans, A.A., Penna, A., Corsi, I., 2020. Impact of polystyrene nanoparticles on marine diatom *Skeletonema marinoi* chain assemblages and consequences on their ecological role in marine ecosystems. *Environ. Pollut.* 262, 114268. <https://doi.org/10.1016/j.envpol.2020.114268>.
- Chae, Y., Kim, D., Kim, S.W., An, Y.-J., 2018. Trophic transfer and individual impact of nano-sized polystyrene in a four-species freshwater food chain. *Sci. Rep.* 8, 284. <https://doi.org/10.1038/s41598-017-18849-y>.
- Dalvit, C., Vulpatti, A., 2016. Weak intermolecular hydrogen bonds with fluorine: detection and implications for enzymatic/chemical reactions, chemical properties, and ligand/protein fluorine NMR screening. *Chem. Eur. J.* 22 (22), 7592–7601. <https://doi.org/10.1002/chem.201600446>.
- Dong, D., Guo, Z., Yang, X., Dai, Y., 2024. Comprehensive understanding of the aging and biodegradation of polystyrene-based plastics. *Environ. Pollut.* 342, 123034. <https://doi.org/10.1016/j.envpol.2023.123034>.
- Duan, Z., Wang, P., Yu, G., Liang, M., Dong, J., Su, J., Huang, W., Li, Y., Zhang, A., Chen, C., 2021. Aggregation kinetics of UV-aged soot nanoparticles in wet environments: Effects of irradiation time and background solution chemistry. *Water Res.* 201, 117385. <https://doi.org/10.1016/j.watres.2021.117385>.
- Gaylarde, C.C., Baptista Neto, J.A., da Fonseca, E.M., 2021. Nanoplastics in aquatic systems - are they more hazardous than microplastics? *Environ. Pollut.* 272, 115950. <https://doi.org/10.1016/j.envpol.2020.115950>.
- Gigault, J., Halle, A., Baudrimont, M., Pascal, P.-Y., Gauffre, F., Phi, T.-L., El Hadri, H., Grassl, B., Reynaud, S., 2018. Current opinion: What is a nanoplastic. *Environ. Pollut.* 235, 1030–1034. <https://doi.org/10.1016/j.envpol.2018.01.024>.
- Hiemstra, T., 2018. Ferrihydrite interaction with silicate and competing oxyanions: Geometry and Hydrogen bonding of surface species. *Geochim. Cosmochim. Acta* 238, 453–476. <https://doi.org/10.1016/j.gca.2018.07.017>.
- Hou, L., Liang, Q., Wang, F., 2020. Mechanisms that control the adsorption-desorption behavior of phosphate on magnetite nanoparticles: the role of particle size and surface chemistry characteristics. *RSC Adv.* 10 (4), 2378–2388. <https://doi.org/10.1039/c9ra08517c>.
- Hu, J.-D., Zevi, Y., Kou, X.-M., Xiao, J., Wang, X.-J., Jin, Y., 2010. Effect of dissolved organic matter on the stability of magnetite nanoparticles under different pH and ionic strength conditions. *Sci. Total Environ.* 408 (16), 3477–3489. <https://doi.org/10.1016/j.scitotenv.2010.03.033>.
- Hu, L., Ren, X., Yang, M., Guo, W., 2021. Facet-controlled activation of persulfate by magnetite nanoparticles for the degradation of tetracycline. *Sep. Purif. Technol.* 258, 118014. <https://doi.org/10.1016/j.seppur.2020.118014>.
- Huang, D., Tao, J., Cheng, M., Deng, R., Chen, S., Yin, L., Li, R., 2021. Microplastics and nanoplastics in the environment: macroscopic transport and effects on creatures. *J. Hazard. Mater.* 407, 124399. <https://doi.org/10.1016/j.jhazmat.2020.124399>.
- Huang, Z., Chen, C., Liu, Y., Liu, S., Zeng, D., Yang, C., Huang, W., Dang, Z., 2022. Influence of protein configuration on aggregation kinetics of nanoplastics in aquatic environment. *Water Res.* 219, 118522. <https://doi.org/10.1016/j.watres.2022.118522>.
- Kong, Y., Li, X., Tao, M., Cao, X., Wang, Z., Xing, B., 2023. Cation- π mechanism promotes the adsorption of humic acid on polystyrene nanoplastics to differently affect their aggregation: Evidence from experimental characterization and DFT calculation. *J. Hazard. Mater.* 459, 132071. <https://doi.org/10.1016/j.jhazmat.2023.132071>.
- Lee, Y.K., Hur, J., 2020. Adsorption of microplastic-derived organic matter onto minerals. *Water Res.* 187, 116426. <https://doi.org/10.1016/j.watres.2020.116426>.
- Lee, W.-H., Kim, J.-O., 2017. Effect of coexisting components on phosphate adsorption using magnetite particles in water. *Environ. Sci. Pollut. Res.* 26 (2), 1054–1060. <https://doi.org/10.1007/s11356-017-8528-1>.
- Li, M., He, L., Zhang, M., Liu, X., Tong, M., Kim, H., 2019. Cotransport and deposition of iron oxides with different-sized plastic particles in saturated quartz sand. *Environ. Sci. Technol.* 53 (7), 3547–3557. <https://doi.org/10.1021/acs.est.8b06904>.
- Li, N., Liu, Y., Du, C., Wang, Y., Wang, L., Li, X., 2023. A novel role of various hydrogen bonds in adsorption, desorption and co-adsorption of PPCPs on corn straw-derived biochars. *Sci. Total Environ.* 861, 160623. <https://doi.org/10.1016/j.scitotenv.2022.160623>.
- Li, X., He, E., Xia, B., Liu, Y., Zhang, P., Cao, X., Zhao, L., Xu, X., Qiu, H., 2021a. Protein corona-induced aggregation of differently sized nanoplastics: impacts of protein type and concentration. *Environ. Sci. -Nano.* 8 (6), 1560–1570. <https://doi.org/10.1039/d1en00115a>.
- Lee, W.-H., Kim, J.-O., 2022. Phosphate recovery from anaerobic digestion effluent using synthetic magnetite particles. *J. Environ. Chem. Eng.* 10 (1), 107103. <https://doi.org/10.1016/j.jece.2021.107103>.
- Li, X., He, E., Jiang, K., Peijnenburg, W.J.G.M., Qiu, H., 2021b. The crucial role of a protein corona in determining the aggregation kinetics and colloidal stability of polystyrene nanoplastics. *Water Res.* 190, 116742. <https://doi.org/10.1016/j.watres.2020.116742>.
- Li, Z., Lowry, G.V., Fan, J., Liu, F., Chen, J., 2018. High molecular weight components of natural organic matter preferentially adsorb onto nanoscale zero valent iron and magnetite. *Sci. Total Environ.* 628–629, 177–185. <https://doi.org/10.1016/j.scitotenv.2018.02.038>.
- Liang, X., Lin, X., Wei, G., Ma, L., He, H., Santos-Carballal, D., Zhu, J., Zhu, R., De Leeuw, N.H., 2021. Competitive adsorption geometries for the arsenate As(V) and phosphate P(V) oxyanions on magnetite surfaces: experiments and theory. *Am. Mineral.* 106 (3), 374–388. <https://doi.org/10.2138/am-2020-7350>.
- Lin, J., Xiang, W., Zhan, Y., 2023. Comparison of magnetite, hematite and goethite amendment and capping in control of phosphorus release from sediment. *Environ. Sci. Pollut. Res.* 30 (24), 66080–66101. <https://doi.org/10.1007/s11356-023-27063-5>.
- Lin, X., Wei, G., Liang, X., Liu, J., Ma, L., Zhu, J., 2021. The competitive adsorption of chromate and sulfate on Ni-substituted magnetite surfaces: an ATR-FTIR study. *Minerals* 11 (1), 88. <https://doi.org/10.3390/min11010088>.
- Lin, X., Nie, X., Xie, R., Qin, Z., Ran, M., Wan, Q., Wang, J., 2024. Heteroaggregation and deposition behaviors of carboxylated nanoplastics with different types of clay minerals in aquatic environments: Important role of calcium(II) ion-assisted bridging. *Ecotoxicol. Environ. Saf.* 280, 116533. <https://doi.org/10.1016/j.ecoenv.2024.116533>.
- Ling, X., Yan, Z., Lu, G., 2022. Vertical transport and retention behavior of polystyrene nanoplastics in simulated hyporheic zone. *Water Res.* 219, 118609. <https://doi.org/10.1016/j.watres.2022.118609>.
- Liu, Y., Huang, Z., Zhou, J., Tang, J., Yang, C., Chen, C., Huang, W., Dang, Z., 2020. Influence of environmental and biological macromolecules on aggregation kinetics of nanoplastics in aquatic systems. *Water Res.* 186, 116316. <https://doi.org/10.1016/j.watres.2020.116316>.
- Mahmudov, K.T., Kopylovich, M.N., Guedes da Silva, M.F.C., Pombeiro, A.J.L., 2017. Non-covalent interactions in the synthesis of coordination compounds: recent advances. *Coord. Chem. Rev.* 345, 54–72. <https://doi.org/10.1016/j.ccr.2016.09.002>.
- Mamun, A.A., Prasetya, T.A.E., Dewi, I.R., Ahmad, M., 2023. Microplastics in human food chains: Food becoming a threat to health safety. *Sci. Total Environ.* 858 (Pt 1), 159834. <https://doi.org/10.1016/j.scitotenv.2022.159834>.

- Manna, S., Saha, P., Roy, D., Sen, R., Adhikari, B., 2015. Defluoridation potential of jute fibers grafted with fatty acyl chain. *Appl. Surf. Sci.* 356, 30–38. <https://doi.org/10.1016/j.apsusc.2015.08.007>.
- Nie, X., Xing, X., Xie, R., Wang, J., Yang, S., Wan, Q., Zeng, E.Y., 2023. Impact of iron/aluminum (hydr)oxide and clay minerals on heteroaggregation and transport of nanoplastics in aquatic environment. *J. Hazard. Mater.* 446, 130649. <https://doi.org/10.1016/j.jhazmat.2022.130649>.
- Rhein, F., Nirschl, H., Kaegi, R., 2022. Separation of Microplastic Particles from Sewage Sludge Extracts Using Magnetic Seeded Filtration. *Water Res. X* 17, 0100155. <https://doi.org/10.1016/j.wroa.2022.100155>.
- Ross, P.D., Rekharsky, M.V., 1996. Thermodynamics of hydrogen bond and hydrophobic interactions in cyclodextrin complexes. *Biophys. J.* 71, 2144–2154. [https://doi.org/10.1016/s0006-3495\(96\)79415-8](https://doi.org/10.1016/s0006-3495(96)79415-8).
- Saavedra, J., Stoll, S., Slaveykova, V.I., 2019. Influence of nanoplastic surface charge on eco-corona formation, aggregation and toxicity to freshwater zooplankton. *Environ. Pollut.* 252, 715–722. <https://doi.org/10.1016/j.envpol.2019.05.135>.
- Safur Rahman, M., Whalen, M., Gagnon, G.A., 2013. Adsorption of dissolved organic matter (DOM) onto the synthetic iron pipe corrosion scales (goethite and magnetite): Effect of pH. *Chem. Eng. J.* 234, 149–157. <https://doi.org/10.1016/j.cej.2013.08.077>.
- Schmidtman, J., Elagami, H., Gilfedder, B.S., Fleckenstein, J.H., Papastavrou, G., Mansfeld, U., Peiffer, S., 2022. Heteroaggregation of PS microplastic with ferrihydrite leads to rapid removal of microplastic particles from the water column. *Environ. Sci. Processes & Impacts* 24 (10), 1782–1789. <https://doi.org/10.1039/d2em00207h>.
- Shao, Z., Su, J., Dong, J., Liang, M., Xiao, J., Liu, J., Zeng, Q., Li, Y., Huang, W., Chen, C., 2022. Aggregation kinetics of polystyrene nanoplastics in gastric environments: effects of plastic properties, solution conditions, and gastric constituents. *Environ. Int.* 170, 107628. <https://doi.org/10.1016/j.envint.2022.107628>.
- Sobhani, Z., Zhang, X., Gibson, C., Naidu, R., Megharaj, M., Fang, C., 2020. Identification and visualisation of microplastics/nanoplastics by Raman imaging (i): down to 100 nm. *Water Res.* 174, 115658. <https://doi.org/10.1016/j.watres.2020.115658>.
- Song, X., Lu, J., Liu, M., Tang, L., Sun, L., Jiang, R., Zhang, L., 2024. Highly selective removal of triarylmethane dyes by molecular switched adsorbents via charge-assisted hydrogen bond. *Chem. Eng. J.* 481, 148714. <https://doi.org/10.1016/j.cej.2024.148714>.
- Vindedahl, A.M., Strehlau, J.H., Arnold, W.A., Penn, R.L., 2016. Organic matter and iron oxide nanoparticles: aggregation, interactions, and reactivity. *Environ. Sci. Nano.* 3 (3), 494–505. <https://doi.org/10.1039/c5en00215j>.
- Wang, J., Zhu, J., Zheng, Q., Wang, D., Wang, H., He, Y., Wang, J., Zhan, X., 2023a. In vitro wheat protoplast cytotoxicity of polystyrene nanoplastics. *Sci. Total Environ.* 882, 163560. <https://doi.org/10.1016/j.scitotenv.2023.163560>.
- Wang, Y., Chen, X., Wang, F., Cheng, N., 2023b. Influence of typical clay minerals on aggregation and settling of pristine and aged polyethylene microplastics. *Environ. Pollut.* 316 (Pt 2), 120649. <https://doi.org/10.1016/j.envpol.2022.120649>.
- Wardrop, P., Shimeta, J., Nugegoda, D., Morrison, P.D., Miranda, A., Tang, M., Clarke, B.O., 2016. Chemical pollutants sorbed to ingested microbeads from personal care products accumulate in fish. *Environ. Sci. Technol.* 50 (7), 4037–4044. <https://doi.org/10.1021/acs.est.5b06280>.
- Wu, J., Jiang, R., Liu, Q., Ouyang, G., 2021. Impact of different modes of adsorption of natural organic matter on the environmental fate of nanoplastics. *Chemosphere* 263, 127967. <https://doi.org/10.1016/j.chemosphere.2020.127967>.
- Xie, R., Xing, X., Nie, X., Ma, X., Wan, Q., Chen, Q., Li, Z., Wang, J., 2023. Deposition behaviors of carboxyl-modified polystyrene nanoplastics with goethite in aquatic environment: Effects of solution chemistry and organic macromolecules. *Sci. Total Environ.* 904, 166783. <https://doi.org/10.1016/j.scitotenv.2023.166783>.
- Xu, Y., Lv, K., Xiong, Z., Leng, W., Du, W., Liu, D., Xue, X., 2007. Rate enhancement and rate inhibition of phenol degradation over irradiated anatase and rutile TiO₂ on the addition of NaF: new insight into the mechanism. *J. Phys. Chem. C* 111 (51), 19024–19032. <https://doi.org/10.1021/jp076364w>.
- Yan, Y., Xu, H., Wang, Z., Chen, H., Yang, L., Sun, Y., Zhao, C., Wang, D., 2024. Effect of surface functional groups of polystyrene micro/nano plastics on the release of NOM from flocs during the aging process. *J. Hazard. Mater.* 472, 134421. <https://doi.org/10.1016/j.jhazmat.2024.134421>.
- Yuan, P., Liu, D., Fan, M., Yang, D., Zhu, R., Ge, F., Zhu, J., He, H., 2010. Removal of hexavalent chromium [Cr(VI)] from aqueous solutions by the diatomite-supported/unsupported magnetite nanoparticles. *J. Hazard. Mater.* 173, 614–621. <https://doi.org/10.1016/j.jhazmat.2009.08.129>.
- Zandieh, M., Liu, J., 2022. Removal and degradation of microplastics using the magnetic and nanozyme activities of bare iron oxide nanoaggregates. *Angew. Chem. Int. Ed.* 61 (47). <https://doi.org/10.1002/anie.202212013>.
- Zhang, C., Li, Y., Wang, T.-J., Jiang, Y., Fok, J., 2017b. Synthesis and properties of a high-capacity iron oxide adsorbent for fluoride removal from drinking water. *Appl. Surf. Sci.* 425, 272–281. <https://doi.org/10.1016/j.apsusc.2017.06.159>.
- Zhang, F., Wang, Z., Wang, S., Fang, H., Wang, D., 2019. Aquatic behavior and toxicity of polystyrene nanoplastic particles with different functional groups: complex roles of pH, dissolved organic carbon and divalent cations. *Chemosphere* 228, 195–203. <https://doi.org/10.1016/j.chemosphere.2019.04.115>.
- Zhang, J., Zhang, C., Wei, G., Li, Y., Liang, X., Chu, W., He, H., Huang, D., Zhu, J., Zhu, R., 2017a. Reduction removal of hexavalent chromium by zinc-substituted magnetite coupled with aqueous Fe(II) at neutral pH value. *J. Colloid Interface Sci.* 500, 20–29. <https://doi.org/10.1016/j.jcis.2017.03.103>.
- Zhang, P., Liu, Y., Zhang, L., Xu, M., Gao, L., Zhao, B., 2022a. The interaction of micro/nano plastics and the environment: effects of ecological corona on the toxicity to aquatic organisms. *Ecotoxicol. Environ. Saf.* 243, 113997. <https://doi.org/10.1016/j.ecoenv.2022.113997>.
- Zhang, Y., Luo, Y., Guo, X., Xia, T., Wang, T., Jia, H., Zhu, L., 2020. Charge mediated interaction of polystyrene nanoplastic (PSNP) with minerals in aqueous phase. *Water Res.* 178, 115861. <https://doi.org/10.1016/j.watres.2020.115861>.
- Zhang, Y., Luo, Y., Yu, X., Huang, D., Guo, X., Zhu, L., 2022b. Aging significantly increases the interaction between polystyrene nanoplastic and minerals. *Water Res.* 219, 118544. <https://doi.org/10.1016/j.watres.2022.118544>.
- Zhao, Y., Geng, J., Wang, X., Gu, X., Gao, S., 2011. Adsorption of tetracycline onto goethite in the presence of metal cations and humic substances. *J. Colloid Interface Sci.* 361 (1), 247–251. <https://doi.org/10.1016/j.jcis.2011.05.051>.
- Zhou, Y., Zhang, Y., Li, P., Li, G., Jiang, T., 2014. Comparative study on the adsorption interactions of humic acid onto natural magnetite, hematite and quartz: effect of initial HA concentration. *Powder Technol.* 251, 1–8. <https://doi.org/10.1016/j.powtec.2013.10.011>.
- Zhou, Y., Zhang, Y., Li, G., Wu, Y., Jiang, T., 2015. A further study on adsorption interaction of humic acid on natural magnetite, hematite and quartz in iron ore pelletizing process: effect of the solution pH value. *Powder Technol.* 271, 155–166. <https://doi.org/10.1016/j.powtec.2014.10.045>.